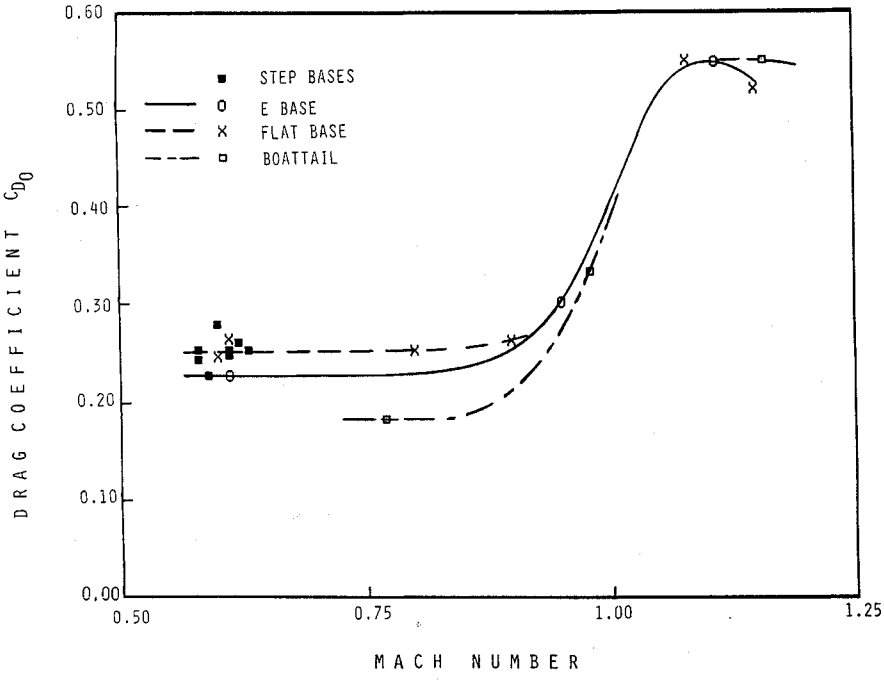

Fig. 3 Zero-angle drag coefficient results for the fin-stabilized projectiles.

Concluding Remarks

Free-flight tests of spin-stabilized projectiles and fin-stabilized missiles with various stepped, flat, and boattailed bases have been conducted at subsonic, transonic, and supersonic Mach numbers. The results indicate that subsonically the addition of a stepped base can significantly reduce the aerodynamic drag over that of a flat base. However, these stepped bases are not as efficient in reducing drag as a standard truncated boattail. Supersonically, these stepped bases have no apparent advantage over that of a flat base. Although the stepped base drag reductions and captive vortices observed in Kentfield's previous low subsonic wind tunnel tests were not realized in the present free-flight tests, significant differences in the test conditions could be the reason. It is suspected that differences in Mach number and Reynolds number were the primary causes. The present tests reaffirm that boattailed bases are the most effective passive drag reduction technique available for typical munitions and missile configurations at their normal flight conditions.

References

[1]Kentfield, J. A. C., "Short Multi-Step, Afterbody Fairings," *Journal of Aircraft*, Vol. 21, No. 5, 1985, pp. 351-352.

[2]Kentfield, J. A. C., "Drag Reduction of Controlled Separated Flows," AIAA Paper 85-1800, Aug. 1985.

[3]Wikoff, D., Cottrell, C. J., and Packard, J. D., "An Examination of Controlled Vortex Drag Using Stepped Afterbodies from $M = 0.5$ to 3.0," AIAA Paper 87-0445, Jan. 1987.

[4]Kidd, J. A., "An Investigation of Drag Reduction Using Stepped Afterbodies," AIAA Paper 89-0333, Jan. 1989.

[5]Kittyle, R. L., Packard, J. D., and Winchenbach, G. L., "Description and Capabilities of the Aeroballistic Research Facility," Air Force Armament Laboratory, Eglin AFB, TR-87-08, May 1987.

[6]Murphy, C. H., "Data Reduction for Free-Flight Spark Ranges," Ballistic Research Laboratory, Aberdeen Proving Ground, Rept. 900, Feb. 1954.

[7]Sabot, S. M., Winchenbach, G. L., and Chapman, G. T., "Comparison of Various Drag Coefficient Expansions Using Polynomials and Splines," *Journal of Spacecraft and Rockets*, Vol. 23, No. 3, 1986, pp. 259-263.

Hypervelocity, Minimum-Radii, Coordinated Turns

Michael E. Tauber*
NASA Ames Research Center, Moffett Field, California

Nomenclature

A	= vehicle reference area
C_D	= drag coefficient
C_{D_0}	= zero-lift drag coefficient
C_L	= lift coefficient
D	= drag
g	= acceleration of gravity
L	= lift
m	= vehicle mass
n	= structural load factor
R_0	= planetary radius (6367 km for Earth)
r_c	= radius of curvature of fligh path
r_t	= radius of turn
T	= thrust
t	= time
V	= flight velocity
V_s	= circular satellite speed (7.9 km/s)
W	= vehicle weight
α	= angle of attack
ρ	= freestream air density
τ	= thrust-to-weight ratio
ϕ	= bank or roll angle

Received May 15, 1989; revision received Oct. 20, 1989.

*Research Scientist. Associate Fellow AIAA.

Introduction

DURING the last few years, we have witnessed a revival of interest in hypervelocity, powered atmospheric flight. A lift drag ratio (L/D) in excess of two and approaching three is required for efficient flight within the atmosphere. Such high L/D offer the potential for performing extensive maneuvers using aerodynamic forces. (For comparison, the Space Shuttle Orbiter has a maximum L/D of slightly less than two.) In the present Note, an analytic solution is presented for the most basic powered-flight maneuver consisting of a constant-altitude coordinated turn and expressions for minimum-turn radii, and the associated flight conditions are derived. It will be shown that the formulation for hypervelocity turns differs from that used for subsonic or supersonic speeds. Some example calculations will be used to illustrate that the turning radii and the corresponding flight conditions are very different from those encountered at lower speeds.

Analysis

For a spherical, nonrotating planet and for flight at a constant altitude with the thrust axis aligned with the vehicle axis, the sum of vertical forces for banked flight gives[1]

$$L\cos = mg - \frac{mV^2}{r_c} - T\sin\alpha\cos\phi \tag{1}$$

For flight within the atmosphere where the altitude is much less than Earth's radius

$$r_c \approx R_o = V_s^2/g \tag{2}$$

resulting in

$$(L + T\sin\alpha)\cos\phi = mg\,(1 - V^2/V_s^2) \tag{3}$$

The expression for the tangential forces, for unaccelerated flight, is

$$D = T\cos\alpha \tag{4}$$

and summing the radial forces yields

$$(L + T\sin\alpha)\sin\phi = \frac{mV^2}{r_t} \tag{5}$$

where the change in the vehicle's mass during the turn has been neglected to a first order of approximation. From Eqs. (3) and (5), the turning radius is

$$r_t = \frac{V^2}{g(1 - V^2/V_s^2)\tan\phi} \tag{6}$$

As $V/V_s \to 0$, Eq. (6) approaches the expression for the turning radius at low speeds.[2] Solving Eq. (3) for velocity and substituting the result into Eq. (6) gives

$$\frac{r_t}{R_o} = \frac{1 - \tau\sin\alpha\cos\phi}{[(C_L A\rho R_o)/2m + \tau\sin\alpha]\sin\phi} \tag{7}$$

where the radius of the turn has been normalized by the Earth's radius and τ is the thrust-to-weight ratio in flight. If we assume that the thrust, weight, and altitude remain constant during the turn, we can find the bank angle giving the minimum-turning radius by differentiating Eq. (7) with respect to ϕ, which yields the same relation that applies at low speeds[2]

$$\cos\phi = \tau\sin\alpha \tag{8}$$

However, the structural-load factor, defined by

$$n = \frac{1}{\cos\phi} = \frac{L + T\sin\alpha}{W(1 - V^2/V_s^2)} \tag{9}$$

may constrain the bank angle. The load-factor limit imposes the requirement [from Eqs. (8) and (9)] that

$$n_{\lim} \geq \frac{1}{\tau\sin\alpha} \tag{10}$$

If Eq. (10) is satisfied, then Eqs. (3), (4), and (8) can be combined to find the velocity and altitude (density) for the coordinated turn of minimum radius to be

$$\frac{V}{V_s} = \left[1 - \left(\frac{L}{D}\cos\alpha + \sin\alpha\right)\tau^2\sin\alpha\right]^{1/2} \tag{11}$$

$$\rho = \frac{2\tau\cos\alpha}{C_D A R_0/m\,[1 - (L/D\cos\alpha + \sin\alpha)\tau^2\sin\alpha]} \tag{12}$$

Substituting Eqs. (11) and (12) into Eq. (7) yields the relation for the minimum-turn radius in terms of τ, L/D, and α, where L/D is a function of α

$$\left(\frac{r_t}{R_0}\right)_{\min} = \frac{1 - (L/D\cos\alpha + \sin\alpha)\tau^2\sin\alpha}{\tau(L/D\cos\alpha + \sin\alpha)[1 - (\tau\sin\alpha)^2]^{1/2}} \tag{13}$$

The aerodynamic characteristics of the vehicle must be known to solve Eq. (13).

To illustrate some results obtained by using the preceding relations, the hypersonic aerodynamics of a winged, flat-bottomed vehicle will be approximated using the Newtonian impact theory. The Newtonian theory models the lift and drag reasonably well at angles of attack equal to or greater than those for maximum L/D where pressure drag is much greater than skin friction.[3] Using the Newtonian theory gives

$$C_L = 2\sin^2\alpha\cos\alpha \tag{14a}$$

$$C_D = 2\sin^3\alpha + C_{D_0} \tag{14b}$$

[These simple relations were checked against a drag polar for the proposed X-20 vehicle at $M = 16$.[4] When the value of C_{D_0} from Ref. 4 was used in Eq. (14b), good agreement was found up to angles of attack near 35 deg.] Now Eqs. (14) can be

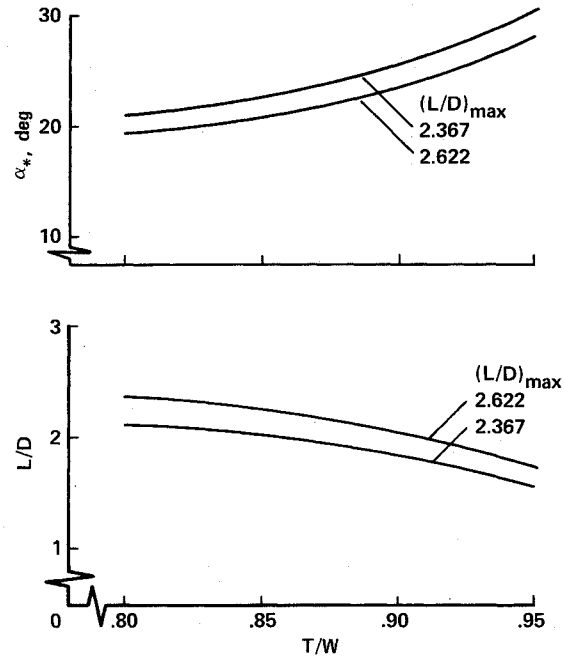

Fig. 1 Aerodynamic values for minimum-radii turns.

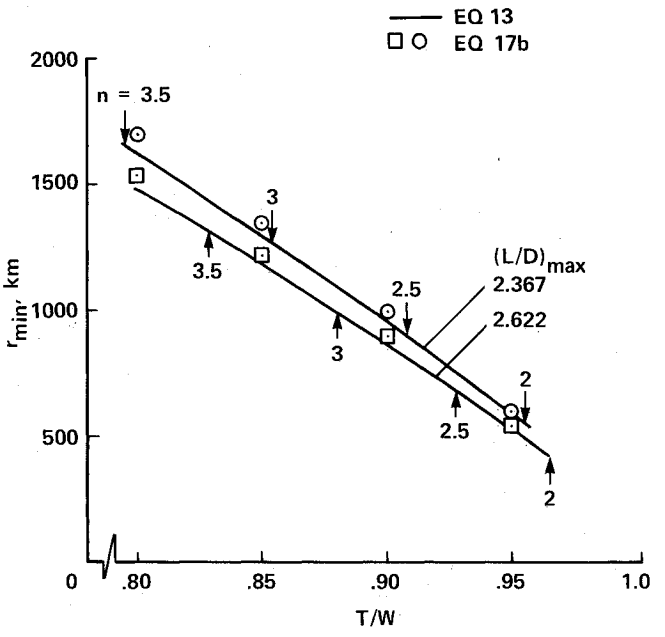

Fig. 2 Minimum turning radii.

substituted into Eq. (13) and, by specifying C_{D_0} and τ, the relation can be evaluated numerically to find the angle of attack α_* and the corresponding L/D, which minimizes the turning radius, subject to the constraint of Eq. (10).

Results and Discussion

Consider two imaginary vehicles whose aerodynamics can be represented by Eqs. (14) having $C_{D_0} = 0.015$ and 0.02; from Eqs. (14), the maximum values of L/D are 2.622 and 2.367, respectively. The simultaneous numerical solution of Eqs. (13) and (14) gives the optimum angles of attack and L/D values (Fig. 1) for thrust-to-weight ratios τ from 0.8 to 0.95. (The choice of these τ values will be discussed.) The optimum angles of attack range from about 20 to 30 deg, whereas the corresponding L/D vary from 90 to roughly 65% of the maximum values, respectively. The minimum turning radii for both vehicles are shown in Fig. 2 and vary from 1480 to 540 km for the lower drag vehicle and from 1620 to 590 km for the higher drag vehicle, as τ increases from 0.8 to about 0.95. Also marked in Fig. 2 are the structural-load factors that vary from over 3.5 to 2 g. In principle, the solution is applicable at lower values of τ; however, the assumption of constant vehicle mass introduces progressively greater errors as the turning radii become larger. Also, as τ decreases, more lift must be used, which causes the load factor to rise. However, a load factor near 3.5 g may be an upper limit for a practical manned vehicle to maintain a low structural weight fraction and for physiological reasons because the turns can last several minutes. (Note that as τ approaches 1, the minimum turning radius approaches zero. This case corresponds to a spiraling, nearly vertical climb that obviously violates the constant-altitude assumption.) The optimum flight speeds and altitudes from Eqs. (11) and (12), corresponding to the minimum turn radii of Fig. 2, are shown in Fig. 3. Speeds vary from 5.3 to 3 km/s, while altitudes are in the neighborhood of 45 km, assuming a wing loading of 300 kg/m^2. Note that the optimum velocity for the turns is independent of the vehicle's aerodynamic characteristics, for the model used here.

More physical insight can be gained by simplifying the aerodynamics even further and making the approximation that

$$\cos\alpha \approx 1 - \frac{\alpha^2}{2}, \qquad \sin\alpha \approx \alpha \tag{15}$$

so that

$$C_L \approx 2\alpha^2\left(1 - \frac{\alpha^2}{2}\right), \qquad C_D \approx 2\alpha^3 + C_{D_0} \tag{16a}$$

from which[3]

$$\left(\frac{L}{D}\right)_{max} \approx \frac{2}{3C_{D_0}^{1/3}} \tag{16b}$$

By applying the approximation of Eq. (15) to Eq. (13) using Eq. (16a), and discarding high-order terms, the angle of attack giving the minimum turning radius α_* is found to be

$$\alpha_* \approx \left(\frac{C_{D_0}}{1-\tau^2}\right)^{1/3} \tag{17a}$$

from which

$$\left(\frac{r_t}{R_0}\right)_{min} \approx \frac{3(1-\tau^2)^{2/3}C_{D_0}^{1/3}}{2\tau} \approx \frac{(1-\tau^2)^{2/3}}{\tau(L/D)_{max}} \tag{17b}$$

where Eq. (16b) was used to write the right-hand side of Eq. (17b). Individual points calculated using the right-hand side of Eq. (17b) are also shown in Fig. 2 and disagree with the previous numerical results by less than 5%. Note the inverse

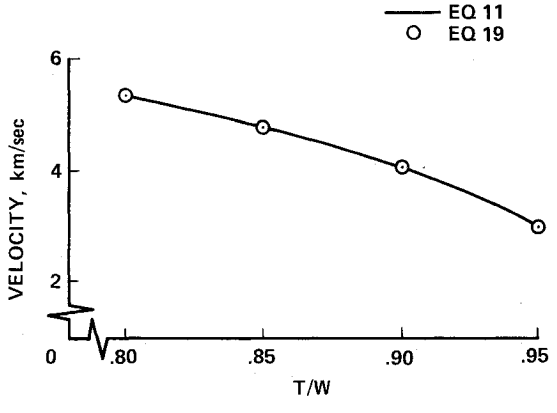

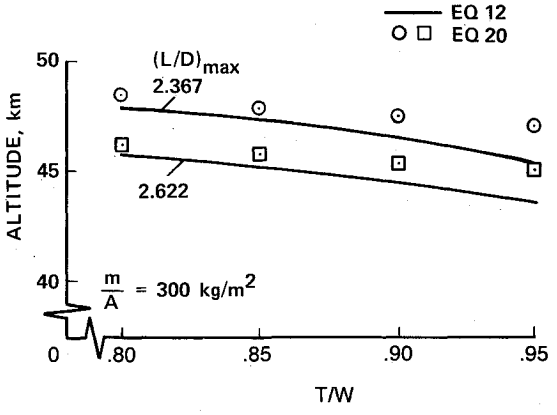

Fig. 3 Flight conditions for minimum-radii turns.

dependence of the minimum turning radius on $(L/D)_{max}$ in Eq. (17b), although the minimum radius turn does not occur at $(L/D)_{max}$ because α_* also depends on τ, as can be seen from Eq. (17a). The inequality of Eq. (10) now becomes

$$\frac{1}{\tau}\left(\frac{1-\tau^2}{C_{D_0}}\right)^{1/3} \leq n_{lim} \tag{18}$$

It is also noteworthy (see Fig. 2) that the tightest turn does not necessarily occur at the limiting load factor, as is the case at low speeds if τ is high enough.[2] Using Eqs. (15) and (17a), the approximate expressions for the flight conditions become

$$\frac{V_*}{V_s} \approx \left[\frac{3(1-\tau^2)}{3-\tau^2}\right]^{1/2} \tag{19}$$

$$\rho_* \approx \frac{2\tau}{3C_{D_0}R_0}\left(\frac{m}{A}\right) \tag{20}$$

The velocity is predicted very well by Eq. (19), while Eq. (20) overpredicts the altitudes by up to 4% (see Fig. 3).

Lastly, the validity of assuming a constant vehicle weight during the turn is examined. Consider the case of a 60 deg turn, or heading change, at a constant 1000-km radius for τ = 0.88. The optimum speed is 4.42 km/s, from Fig. 3, which gives a time of 237 s, or nearly 4 min. Assuming an efficient, air-breathing propulsion system with a specific impulse of 2000 s gives a fuel consumption equal to 10% of the vehicle's weight at the inception of a 60 deg turn. While the vehicle's weight change during a turn is not negligible, the assumption of constant weight made here can be justified on the basis that the present, simplified analysis provides physical insight that is absent in numerical calculations.

Conclusions

An analytic formulation for the case of coordinated, constant altitude and speed, minimum-radius, hypervelocity turns is presented. Some example calculations, performed using approximate aerodynamics based on Newtonian theory, lead to the following conclusions: 1) at hypervelocity speeds, turning radii are very large, typically 500–1500 km; 2) the optimum, constant flight velocities are high, ranging from 3 to 5 km/s; 3) the maneuver must be performed at high altitudes, near 45 km for a wing loading of 300 kg/m^2; 4) large in-flight values of thrust-to-weight ratio are required, in the vicinity of 0.8 to 0.9; 5) the minimum turning radius is inversely proportional to the vehicle's maximum L/D, although the maneuver is not performed at maximum L/D; and 6) in contrast to low-speed turns, the tightest hypervelocity turns are not necessarily performed at the limiting load factor.

Acknowledgment

The author thanks his colleague, D. B. Kirk, for reviewing the paper and making valuable comments.

References

[1]Vinh, N. X., Busemann, A., and Culp, R. D., *Hypersonic and Planetary Entry Flight Mechanics,* University of Michigan, Ann Arbor, MI, 1980.

[2]Dommasch, D. O., Sherby, S. S., and Connolly, T. F., *Airplane Aerodynamics*, 2nd ed., Pitman, New York, 1957.

[3]Tauber, M. E., "Hypersonic Maximum Lift/Drag Ratio of Flat Plates with Bluntness and Skin Friction," NASA TM-88338, July 1986.

[4]"Glider Performance Characteristics Report," Boeing Co., New York, Document D2-8080-1, 1963.

Comparison of High-Angle-of-Attack Slender-Body Theory and Exact Solutions for Potential Flow Over an Ellipsoid

Michael J. Hemsch*
Lockheed Engineering and Sciences Co., Hampton, Virginia 23666

Nomenclature

a	= half-length of ellipsoid
b	= half-span of ellipsoid
C_{NL}	= longitudinal distribution of the normal-force coefficient
C_{YL}	= longitudinal distribution of the side-force coefficient
C_p	= pressure coefficient
c	= half-height of ellipsoid
L	= body length
M_∞	= Mach number
r_0	= radius of transformed cross section in the circle plane
$S(x)$	= axial distribution of cross-sectional area
W	= complex velocity potential, $\phi + i\psi$
u, v, w	= Cartesian velocity components in body-axis coordinates (see Fig. 1)
α	= angle of attack
β	= angle of sideslip
ϵ_{max}	= maximum percent error in C_{NL}
θ	= angle between crossflow velocity vector and z axis
ν	= complex position in transform (circle) plane
σ	= complex position in physical plane
ϕ	= velocity potential
ψ	= stream function

Subscripts

$2D,\alpha$	= two-dimensional solution for crossflow (doublet)
$2D,t$	= two-dimensional solution for thickness (source)
$2D,B$	= two-dimensional solution for thickness (source) for circular body with cross-sectional area $S(x)$
axi	= axisymmetric solution for equivalent body
long	= longitudinal flow

Introduction

IT is generally assumed that the subsonic/transonic/supersonic slender-body theory of Munk,[1] Jones,[2] Ward,[3] and Spreiter[4] applies only to flows about airframes at small angles of attack. However, Barnwell[5] has recently shown that the theory holds for high angles of attack as well, provided that Sychev[6] scaling is used for the flow variables and $M_\infty \sin\alpha \ll 1$. The purpose of this Note is to demonstrate the accuracy of high-angle-of-attack slender-body theory (HASBT) for bodies with elliptical cross sections by comparison with exact solutions for incompressible, potential flow over an ellipsoid.

High-Angle-of-Attack Slender-Body Theory

Heaslet and Spreiter[7] have presented a three-dimensional composite solution for classic slender-body theory (see also

Received Oct. 21, 1989; revision received Dec. 8, 1989.

*Engineer, staff. Associate Fellow AIAA.